CHAPTER – 4

VIBRATIONAL SPECTROSCOPIC INVESTIGATION AND NORMAL COORDINATE ANALYSIS OF THE FIBRATE HYPOLIPIDEMIC AGENT 5-(2, 5-DIMETHYLPHENOXY)-2,2-DIMETHYL PENTANOIC ACID (GEMFIBROZIL)

Fibrates evince greater interest among researchers recently owing to its novel medicinal values. Fibrates are commonly used to reduce major coronary events and increase high-density lipoprotein cholesterol (HDL-C) levels without significant toxicity [85]. Gemfibrozil, chemically known as 2,2-dimethyl-5(2,5 xylyloxy)-valeric acid, also known as 5-(2,5-dimethylphenoxy)-2,2-dimethyl pentanoic acid [86], a member of the fibrate class of drugs. The efficacy in the treatment of diabetic dyslipidaemia using this fibric acid derivative has been well established [87-93]. Also it is effective in lowering plasma triglycerides in rats, mice and rhesus monkeys [86]. This fibrate hypolipidemic agent is clinically effective in reducing serum cholesterol, triglyceride levels and lowers the incidence of coronary heart disease in humans [94]. Both the triglyceride level and the insulin resistance were decreased concomitantly by treating hypertriglyceridaemic patients with the lipid-lowering fibrate gemfibrozil [90].

In the asymmetric unit of the monoclinic unit cell, there are two independent molecules linked by hydrogen bonds between the carboxylic acid groups and related to each other by a pseudo-two fold axis [95]. Ab initio density functional theory (DFT) computations have become an efficient tool in the prediction of molecular structure, harmonic force fields, vibrational wavenumbers as well as the IR and Raman intensities of pharmaceutically important molecules. The theoretical analysis of gemfibrozil based on HF method has been reported [96] earlier. In this work, detailed vibrational and electronic structure theory studies of 5-(2,5-

dimethylphenoxy)-2,2-dimethyl pentanoic acid have been performed using the scaled quantum mechanical force field technique based on DFT calculations. Natural bond orbital (NBO) analysis has been performed to understand the molecular information such as electron delocalization and intramolecular charge transfer (ICT) of gemfibrozil.

4.1 Experimental details

4.1.1 Sample preparation

The compound gemfibrozil was kindly provided by Beckman Research Institute and city of Hope National Medical Center, Durate, USA. The sample was recrystallized by slow evaporation method using water-methanol (1:1) solutions. Colorless crystals grew from the solution within a day.

4.1.2 IR and Raman measurements

The Fourier-transform infrared spectrum of the title compound prepared with the standard KBr pellet technique is recorded in the region 4000 − 450 cm^{-1} using Perkin Elmer-Paragon 500 FTIR spectrometer with a spectral resolution of 4 cm^{-1}. The FT-Raman spectrum of a solid sample is recorded on a Bruker RFS 100/S Spectrometer in the region 4000 − 50 cm^{-1} at a spectral resolution of 4.0 cm^{-1}. An air-cooled Nd: YAG laser at 1064 nm with an output of 150 mW was used as an exciting source and with a Ge detector.

4.2 Optimized geometries

The molecular geometry, harmonic force field and vibrational frequencies have been computed using the B3LYP/6-31G* basis set with the Gaussian 03 software [97]. The optimized structural parameters of gemfibrozil are compared with the XRD data [95] and listed in Tables 4.1 and 4.2, in accordance with the atom numbering scheme in Fig. 4.1. The calculated C–C bond lengths of the ring vary from

1.39 – 1.41 Å. The ring losses its symmetry owing to strong conjugation of electron donating methyl groups with the ring π system. Methyl groups attached to the phenyl ring are oriented in the same plane.

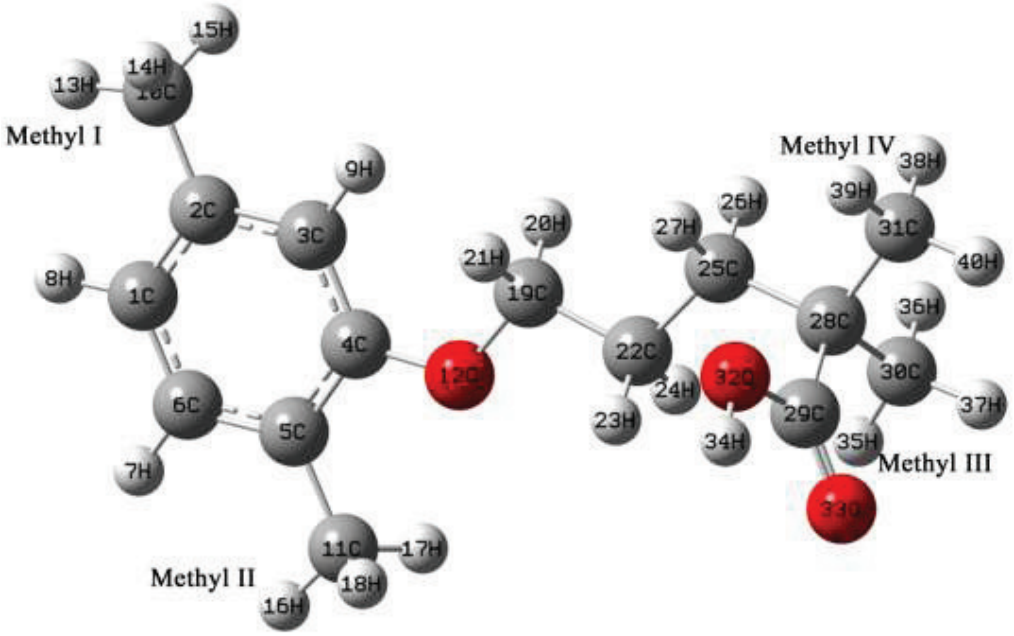

Fig. 4.1 Optimized molecular structure and atomic numbering of gemfibrozil.

The intramolecular contacts $H_{20}\cdots O_{12}$ and $H_{21}\cdots O_{12}$ occur with H···O distances of 2.052 and 2.051 Å respectively, which are significantly shorter than the van der Walls separation between the O atom and H atom (2.72 Å) [98] indicating the existence of the intramolecular C−H···O hydrogen bonding interaction in gemfibrozil. The bond length $C_{29}-O_{33}$ (1.209 Å) is smaller when compared with $C_{29}-O_{32}$ (1.298 Å) infers that the π electrons tend to be mostly localized in the vicinity of $C_{29}-O_{33}$ bond. The $C_{29}-O_{32}$ bond length of 1.361 Å and $O_{32}-H_{34}$ of 0.975 Å is slightly larger than the experimental value and this is caused by the intermolecular hydrogen bonding in crystalline state.

Table 4.1 Selected bond lengths and bond angles of gemfibrozil by B3LYP/6-31G (d) in comparison with the XRD data.

Bond length	Calc. (Å)	Expt. [95] (Å)	Bond angle	Calc. (°)	Expt. [95] (°)
C_1–C_2	1.393	1.391	C_2–C_1–C_6	120.34	121.97
C_6–C_1	1.399	1.365	C_2–C_1–H_8	119.85	118.96
C_1–H_8	1.087	0.929	C_6–C_1–H_8	119.80	119.08
C_2–C_3	1.405	1.402	C_1–C_2–C_3	118.56	116.21
C_2–C_{10}	1.511	1.513	C_1–C_2–C_{10}	121.44	123.54
C_3–C_4	1.395	1.367	C_3–C_2–C_{10}	119.98	120.25
C_3–H_9	1.085	0.930	C_2–C_3–C_4	120.72	122.28
C_4–C_5	1.412	1.401	C_2–C_3–H_9	118.89	118.88
C_4–O_{12}	1.370	1.368	C_4–C_3–H_9	120.37	118.85
C_5–C_6	1.392	1.386	C_3–C_4–C_5	120.95	120.49
C_5–C_{11}	1.507	1.489	C_3–C_4–O_{12}	124.07	123.63
C_6–H_7	1.087	0.929	C_5–C_4–O_{12}	114.96	115.88
C_{10}–H_{13}	1.094	0.958	C_4–C_5–C_6	117.48	117.49
C_{10}–H_{14}	1.097	0.961	C_4–C_5–C_{11}	120.20	120.40
C_{10}–H_{15}	1.097	0.960	C_6–C_5–C_{11}	122.31	122.11
C_{11}–H_{16}	1.094	0.961	C_1–C_6–C_5	121.92	121.56
C_{11}–H_{17}	1.096	0.959	C_1–C_6–H_7	119.42	119.27
C_{11}–H_{18}	1.096	0.960	C_5–C_6–H_7	118.64	119.17
O_{12}–C_{19}	1.423	1.420	C_2–C_{10}–H_{13}	111.27	109.50
C_{19}–H_{20}	1.100	0.970	C_2–C_{10}–H_{14}	111.49	109.46
C_{19}–H_{21}	1.100	0.970	C_2–C_{10}–H_{15}	111.53	109.37
C_{19}–C_{22}	1.524	1.495	H_{13}–C_{10}–H_{14}	107.64	109.57
C_{22}–H_{23}	1.097	0.970	H_{13}–C_{10}–H_{15}	107.69	109.52
C_{22}–H_{24}	1.095	0.970	H_{14}–C_{10}–H_{15}	106.96	109.39
C_{22}–C_{25}	1.534	1.521	C_5–C_{11}–H_{16}	110.78	109.44
C_{25}–C_{28}	1.553	1.544	H_{17}–C_{11}–H_{18}	106.38	109.52
C_{28}–C_{29}	1.530	1.505	C_4–O_{12}–C_{19}	119.15	117.28
C_{28}–C_{30}	1.537	1.535	O_{12}–C_{19}–H_{20}	109.99	109.65
C_{28}–C_{31}	1.547	1.529	O_{12}–C_{19}–H_{21}	110.09	109.71
C_{29}–O_{32}	1.361	1.298	O_{12}–C_{19}–C_{22}	107.58	110.00
C_{29}–O_{33}	1.211	1.209	H_{20}–C_{19}–H_{21}	107.71	108.14
C_{30}–H_{35}	1.093	0.959	H_{20}–C_{19}–C_{22}	110.76	109.65
C_{30}–H_{36}	1.096	0.960	H_{21}–C_{19}–C_{22}	110.69	109.66
C_{30}–H_{37}	1.093	0.960	C_{19}–C_{22}–H_{24}	108.27	109.80
C_{31}–H_{38}	1.096	0.960	C_{28}–C_{29}–O_{32}	112.27	115.45
C_{31}–H_{39}	1.093	0.960	C_{28}–C_{29}–O_{33}	126.13	123.25
C_{31}–H_{40}	1.095	0.959	O_{32}–C_{29}–O_{33}	121.57	121.30
O_{32}–H_{34}	0.975	0.821	C_{29}–O_{32}–H_{34}	105.70	109.45

Table 4.2 Selected dihedral angles of gemfibrozil by B3LYP/6-31G (d) in comparison with the XRD data.

Dihedral angle	Calc. (°)	Expt. [95] (°)
C_6–C_1–C_2–C_{10}	-179.84	-179.24
H_8–C_1–C_2-C_3	-179.94	-179.54
C_1–C_2–C_{10}–H_{14}	117.99	126.14
C_1–C_2–C_{10}–H_{15}	-122.49	-114.03
C_3–C_2–C_{10}–H_{14}	-61.86	-53.55
C_3–C_2–C_{10}–H_{15}	57.65	66.28
C_2–C_3–C_4–O_{12}	-179.94	-179.97
H_9–C_3–C_4–C_5	-179.92	179.82
C_3–C_4–C_5–C_{11}	179.86	178.62
O_{12}–C_4–C_5–C_6	179.96	-179.73
C_3–C_4–O_{12}–C_{19}	-0.34	-1.55
C_4–C_5–C_6–C_1	0.02	-0.32
C_4–C_5–C_6–H_7	179.97	179.73
C_{11}–C_5–C_6–C_1	-179.90	178.80
C_4–C_5–C_{11}–H_{16}	179.92	177.05
C_4–O_{12}–C_{19}–H_{21}	59.14	59.61
C_4–O_{12}–C_{19}–C_{22}	179.84	179.68
O_{12}–C_{19}–C_{22}–H_{23}	-59.39	-56.74
O_{12}–C_{19}–C_{22}–H_{24}	56.12	62.18
H_{20}–C_{19}–C_{22}–H_{23}	-179.64	-177.41
H_{20}–C_{19}–C_{22}–H_{24}	-64.13	-58.49
H_{20}–C_{19}–C_{22}–C_{25}	58.39	62.07
H_{21}–C_{19}–C_{22}–C_{25}	-61.01	-56.53
C_{19}–C_{22}–C_{25}–H_{26}	-61.39	-53.55
C_{19}–C_{22}–C_{25}–H_{27}	54.95	62.18
H_{23}–C_{22}–C_{25}–C_{28}	56.74	63.85
H_{24}–C_{22}–C_{25}–H_{26}	59.56	66.97
H_{24}–C_{22}–C_{25}–H_{27}	175.91	-177.31
H_{24}–C_{22}–C_{25}–C_{28}	-61.61	-55.16
C_{31}–C_{28}–C_{29}–O_{32}	65.79	58.54
C_{31}–C_{28}–C_{29}–O_{33}	-113.27	-121.58
C_{25}–C_{28}–C_{30}–H_{35}	-63.06	-57.76
C_{25}–C_{28}–C_{30}–H_{36}	57.62	62.25
C_{28}–C_{29}–O_{32}–H_{34}	-178.93	-178.75

The decrease in the *endo* angles C_1–C_2–C_3 and C_4–C_5–C_6 (116.21º and 117.49º respectively) and the corresponding increase in the *endo* angles C_2–C_1–C_6, C_1–C_6–C_5 and C_2–C_3–C_4 (121.97º, 121.56º and 122.28º respectively) from the typical

hexagonal angle is due to the attachment of electron donating methyl groups to the phenyl ring. The decrease in the angles $O_{12}-C_{19}-H_{20}$ and $O_{12}-C_{19}-H_{21}$ is due to the intramolecular C−H···O ($C_{19}-H_{20}\cdots O_{12}$ and $C_{19}-H_{21}\cdots O_{12}$) interactions. The largest deviation in the bond angles $C_{28}-C_{29}-O_{32}$ and $C_{29}-O_{32}-H_{34}$ from the theoretical values is attributed to the intermolecular hydrogen bonding O−H···O in the crystal structure of gemfibrozil.

4.3 NBO analysis

The Natural bond orbital analysis provides an efficient method for studying intra- and inter-molecular bonding and interaction among bonds, and also provides a convenient basis for investigating charge transfer or conjugative interaction in molecular systems. Larger the stabilization energy E(2) value, the interaction between electron donors and electron acceptors is more intensive and greater the extent of conjugation of the whole system. The intramolecular hyperconjugative interactions are formed by the orbital overlap between π(C−C) and geminal π*(C−C) bond orbitals which results intramolecular charge transfer (ICT) causing stabilization of the system are presented in Table 4.3.

NBO analysis reveals the charge transfer interaction between the electron donating methyl groups and the geminal σ*(C−C) orbitals. The π-electron delocalization is maximum around the C_1-C_2, C_3-C_4, C_5-C_6 of the phenyl ring which is revealed by the ED at the three conjugated π bonds (~1.69e) and π* bonds (~0.34e). The most important interaction energy related to the resonance in the molecule, is electron donation from $n_2(O)_{12}$ to the antibonding acceptor $\pi^*(C_3-C_4)$ of the phenyl ring (29.73 kcal / mol). This enhanced $\pi^*(C_3-C_4)$ NBO further conjugates with $\pi^*(C_1-C_2)$ and $\pi^*(C_5-C_6)$ resulting to an enormous stabilization energy of 212.31 and

217.35 kcal / mol respectively. The intramolecular C−H···O hydrogen bonds are exposed by the interactions between the oxygen lone-pair $n_2(O)_{12}$ and the antibonding orbitals $\sigma^*(C_{19}-H_{20})$ and $\sigma^*(C_{19}-H_{21})$ whose contribution (5.38 and 5.31 kcal/mol) are smaller but definitely not negligible and can be used as a measure of intramolecular delocalization.

Table 4.3 Second order perturbation theory analysis of Fock matrix in NBO basis.

Donor (i)	ED (i) (e)	Acceptor (j)	ED (j) (e)	E(2)[a] (Kcalmol^{-1})
$\pi(C_1–C_2)$	1.68658	$\pi^*(C_3–C_4)$	0.38134	17.01
		$\pi^*(C_5–C_6)$	0.33180	21.43
$\pi(C_3–C_4)$	1.69205	$\pi^*(C_1–C_2)$	0.34421	21.31
		$\pi^*(C_5–C_6)$	0.33180	16.41
$\pi(C_5–C_6)$	1.69805	$\pi^*(C_1–C_2)$	0.34421	17.57
		$\pi^*(C_3–C_4)$	0.38134	21.42
$\sigma(C_{10}–H_{13})$	1.99107	$\sigma^*(C_2–C_3)$	0.02222	3.94
$\sigma(C_{10}–H_{14})$	1.98212	$\pi^*(C_1–C_2)$	0.34421	3.15
$\sigma(C_{10}–H_{15})$	1.98300	$\pi^*(C_1–C_2)$	0.34421	2.86
$\sigma(C_{11}–H_{16})$	1.99023	$\sigma^*(C_4–C_5)$	0.03030	4.16
$\sigma(C_{11}–H_{17})$	1.98138	$\pi^*(C_5–C_6)$	0.33180	3.05
$\sigma(C_{11}–H_{18})$	1.98146	$\pi^*(C_5–C_6)$	0.33180	3.05
$n_1(O_{12})$	1.96156	$\sigma^*(C_3–C_4)$	0.02506	6.83
$n_2(O_{12})$	1.84523	$\pi^*(C_3–C_4)$	0.38134	29.73
		$\sigma^*(C_{19}–H_{20})$	0.02680	5.38
		$\sigma^*(C_{19}–H_{21})$	0.02662	5.31
$n_1(O_{32})$	1.97645	$\sigma^*(C_{29}–O_{33})$	0.02160	6.92
$\sigma(C_{30}–H_{36})$	1.98850	$\sigma^*(C_{28}–C_{29})$	0.07709	3.06
$\sigma(C_{31}–H_{38})$	1.98731	$\sigma^*(C_{28}–C_{29})$	0.07709	2.90
$n_2(O_{33})$	1.84637	$\sigma^*(C_{28}–C_{29})$	0.07709	19.61
		$\sigma^*(C_{29}–O_{32})$	0.10265	34.27
$\pi^*(C_3–C_4)$	0.38134	$\pi^*(C_1–C_2)$	0.34421	212.31
		$\pi^*(C_5–C_6)$	0.33180	217.35

[a] E(2) means energy of hyperconjugative interactions.

4.4 Vibrational analysis

Gemfibrozil consists of 40 atoms, which has 114 normal modes of vibration. These modes of gemfibrozil have been assigned according to the detailed vibrations of the individual atoms. Internal valence coordinates of the title compound has been defined in Table 4.4. Force constants of the symmetry coordinates and the scale factors used are given in Table 4.5. Fig. 4.2 and Fig. 4.3 present the FT-IR and FT-Raman spectra of the molecule respectively. The experimental FT-IR and FT-Raman together with the calculated wavenumbers are tabulated (Table 4.6).

Table 4.4 Definition of internal valence coordinates of gemfibrozil.

No	Symbol	Type	Definition
Stretching			
1-6	R_i	C-C (ring)	C_1-C_2, C_2-C_3, C_3-C_4, C_4-C_5, C_5-C_6, C_6-C_1
7-9	r_i	C-H (ring)	C_1-H_8, C_3-H_9, C_6-H_7
10-11	r_i	C-C (methyl)	C_2-C_{10}, C_5-C_{11}
12-23	r_i	C-H (methyl)	C_{10}-H_{13}, C_{10}-H_{14}, C_{10}-H_{15}, C_{11}-H_{16}, C_{11}-H_{17}, C_{11}-H_{18}, C_{30}-H_{35}, C_{30}-H_{36}, C_{30}-H_{37}, C_{31}-H_{38}, C_{31}-H_{39}, C_{31}-H_{40}
24-29	r_i	C-H (methylene)	C_{19}-H_{20}, C_{19}-H_{21}, C_{22}-H_{23}, C_{22}-H_{24}, C_{25}-H_{26}, C_{25}-H_{27}
30	Q_i	C-O (ring)	C_4-O_{12}
31	Q_i	O-C (chain)	O_{12}-C_{19}
32-37	R_i	C-C (chain)	C_{19}-C_{22}, C_{22}-C_{25}, C_{25}-C_{28}, C_{28}-C_{29}, C_{28}-C_{30}, C_{28}-C_{31}
38	R_i	C-O (carboxylic)	C_{29}-O_{32}
39	Q_i	C=O (carboxylic)	C_{29}=O_{33}
40	P_i	O-H (carboxylic)	O_{32}-H_{34}
Bending			
41-46	β_i	C-C-H (ring)	C_2-C_3-H_9, C_4-C_3-H_9, C_2-C_1-H_8, C_6-C_1-H_8, C_5-C_6-H_7, C_1-C_6-H_7
47-52	δ_i	C-C-C (ring)	C_5-C_4-C_3, C_3-C_2-C_1, C_1-C_6-C_5, C_4-C_3-C_2, C_2-C_1-C_6, C_6-C_5-C_4
53-56	α_i	C-C-C (methyl)	C_3-C_2-C_{10}, C_1-C_2-C_{10}, C_4-C_5-C_{11}, C_6-C_5-C_{11}
57-68	α_i	H-C-H (methyl)	H_{13}-C_{10}-H_{14}, H_{13}-C_{10}-H_{15}, H_{14}-C_{10}-H_{15}, H_{18}-C_{11}-H_{16}, H_{18}-C_{11}-H_{17}, H_{17}-C_{11}-H_{16}, H_{37}-C_{30}-

No	Symbol	Type	Definition
			H_{36}, H_{37}-C_{30}-H_{35}, H_{36}-C_{30}-H_{35}, H_{38}-C_{31}-H_{39}, H_{38}-C_{31}-H_{40}, H_{39}-C_{31}-H_{40}
69-80	β_i	C-C-H (methyl)	C_2-C_{10}-H_{13}, C_2-C_{10}-H_{14}, C_2-C_{10}-H_{15}, C_5-C_{11}-H_{16}, C_5-C_{11}-H_{17}, C_5-C_{11}-H_{18}, C_{28}-C_{30}-H_{35}, C_{28}-C_{30}-H_{36}, C_{28}-C_{30}-H_{37}, C_{28}-C_{31}-H_{38}, C_{28}-C_{31}-H_{39}, C_{28}-C_{31}-H_{40}
81-86	α_i	C-C-C(carboxylic)	C_{31}-C_{28}-C_{30}, C_{29}-C_{28}-C_{31}, C_{30}-C_{28}-C_{29}, C_{25}-C_{28}-C_{29}, C_{25}-C_{28}-C_{30}, C_{25}-C_{28}-C_{31}
87-88	β_i	C-C-O (ring)	C_3-C_4-O_{12}, C_5-C_4-O_{12}
89		C-O-C (chain)	C_4-O_{12}-C_{19}
90-92	α_i	H-C-H (methylene)	H_{20}-C_{19}-H_{21}, H_{23}-C_{22}-H_{24}, H_{27}-C_{25}-H_{26}
93	γ_i	C-C-O (methylene)	C_{22}-C_{19}-O_{12}
94-95	β_i	O-C-H (methylene)	O_{12}-C_{19}-H_{20}, O_{12}-C_{19}-H_{21}
96-97	γ_i	C-C-C (methylene)	C_{19}-C_{22}-C_{25}, C_{22}-C_{25}-C_{28}
98-107	β_i	C-C-H (methylene)	C_{22}-C_{19}-H_{21}, C_{22}-C_{19}-H_{20}, C_{19}-C_{22}-H_{23}, C_{19}-C_{22}-H_{24}, C_{25}-C_{22}-H_{23}, C_{25}-C_{22}-H_{24}, C_{28}-C_{25}-H_{26}, C_{28}-C_{25}-H_{27}, C_{22}-C_{25}-H_{26}, C_{22}-C_{25}-H_{27}
108	Φ_i	O-C-O (carboxylic)	O_{33}-C_{29}-O_{32}
109	Φ_i	C-C-O (carboxylic)	C_{28}-C_{29}-O_{32}
110	Φ_i	O-C-C (carboxylic)	O_{33}-C_{29}-C_{28}
111	α_i	H-O-C (carboxylic)	H_{34}-O_{32}-C_{29}
Out-of-Plane bending (wagging)			
112-114	ω_i	C-H (ring)	H_7-C_6-C_5-C_1, H_8-C_1-C_2-C_6, H_9-C_3-C_2-C_4
115-116	ω_i	C-C (ring)	C_{10}-C_2-C_1-C_3, C_{11}-C_5-C_4-C_6
117	ω_i	O-C (chain)	O_{12}-C_4-C_3-C_5
118	ω_i	C-O (carboxylic)	O_{33}-C_{29}-O_{32}-C_{28}
Torsion			
119-124	τ_i	tC-C (ring)	C_6-C_5-C_4-C_3, C_5-C_4-C_3-C_2, C_4-C_3-C_2-C_1, C_3-C_2-C_1-C_6, C_2-C_1-C_6-C_5, C_1-C_6-C_5-C_4
125-154	τ_i	tC-CH3	H_{13}-C_{10}-C_2-C_3, H_{14}-C_{10}-C_2-C_3, H_{15}-C_{10}-C_2-C_3, H_{13}-C_{10}-C_2-C_1, H_{14}-C_{10}-C_2-C_1, H_{15}-C_{10}-C_2-C_1, H_{16}-C_{11}-C_5-C_4, H_{17}-C_{11}-C_5-C_4, H_{18}-C_{11}-C_5-C_4, H_{16}-C_{11}-C_5-C_6, H_{17}-C_{11}-C_5-C_6, H_{18}-C_{11}-C_5-C_6, H_{35}-C_{30}-C_{28}-C_{25}, H_{36}-C_{30}-C_{28}-C_{25}, H_{37}-C_{30}-C_{28}-C_{25}, H_{35}-C_{30}-C_{28}-C_{29}, H_{36}-C_{30}-C_{28}-C_{29}, H_{37}-C_{30}-C_{28}-C_{29}, H_{35}-C_{30}-

No	Symbol	Type	Definition
			C_{28}-C_{31}, H_{36}-C_{30}-C_{28}-C_{31}, H_{37}-C_{30}-C_{28}-C_{31}, H_{38}-C_{31}-C_{28}-C_{25}, H_{39}-C_{31}-C_{28}-C_{25}, H_{40}-C_{31}-C_{28}-C_{25}, H_{38}-C_{31}-C_{28}-C_{29}, H_{39}-C_{31}-C_{28}-C_{29}, H_{40}-C_{31}-C_{28}-C_{29}, H_{38}-C_{31}-C_{28}-C_{30}, H_{39}-C_{31}-C_{28}-C_{30}, H_{40}-C_{31}-C_{28}-C_{30}
155-163	τ_i	tC-CH3 (carboxylic)	C_{30}-C_{28}-C_{25}-H_{26}, C_{30}-C_{28}-C_{25}-H_{27}, C_{30}-C_{28}-C_{25}-C_{22}, C_{31}-C_{28}-C_{25}-H_{26}, C_{31}-C_{28}-C_{25}-H_{27}, C_{31}-C_{28}-C_{25}-C_{22}, C_{29}-C_{28}-C_{25}-H_{26}, C_{29}-C_{28}-C_{25}-H_{27}, C_{29}-C_{28}-C_{25}-C_{22}
164-165	τ_i	tC-O (chain)	C_{19}-O_{12}-C_4-C_3, C_{19}-O_{12}-C_4-C_5
166-180	τ_i	tC-CH2	H_{20}-C_{19}-O_{12}-C_4, H_{21}-C_{19}-O_{12}-C_4, C_{22}-C_{19}-O_{12}-C_4, H_{23}-C_{22}-C_{19}-O_{12}, H_{24}-C_{22}-C_{19}-O_{12}, C_{25}-C_{22}-C_{19}-O_{12}, H_{20}-C_{19}-C_{22}-C_{25}, H_{21}-C_{19}-C_{22}-C_{25}, O_{12}-C_{19}-C_{22}-C_{25}, H_{26}-C_{25}-C_{22}-C_{19}, H_{27}-C_{25}-C_{22}-C_{19}, H_{28}-C_{25}-C_{22}-C_{19}, H_{23}-C_{22}-C_{25}-C_{28}, H_{24}-C_{22}-C_{25}-C_{28}, C_{19}-C_{22}-C_{25}-C_{28},
181-186	τ_i	tC-C (carboxylic)	O_{33}-C_{29}-C_{28}-C_{25}, O_{33}-C_{29}-C_{28}-C_{30}, O_{33}-C_{29}-C_{28}-C_{31}, O_{32}-C_{29}-C_{28}-C_{25}, O_{32}-C_{29}-C_{28}-C_{30}, O_{32}-C_{29}-C_{28}-C_{31}
187-188	τ_i	tO-H	H_{34}-O_{32}-C_{29}-C_{28}, H_{34}-O_{32}-C_{29}-O_{33}

4.4.1 Phenyl ring vibrations

The assignments of phenyl ring vibrations are made according to Wilson's numbering convention [99]. The C–H stretching vibrations of aromatic ring are observed around 3100 – 3000 cm^{-1}. Hence the bands observed in the Raman spectrum at 3068, 3045 and 3022 cm^{-1} are assigned to C–H stretching vibration of gemfibrozil. The selection rule for asymmetric trisubstituted phenyl ring allows five C–C stretching modes: 8a, 8b, 19a, 19b and 14. The band at 1612 cm^{-1} in Raman is assigned to ring breathing mode 8a. Normal Coordinate Analysis results predict that 1587 cm^{-1} is assigned to ring breathing mode 8b and it is 1586 cm^{-1} in experimental IR spectra. The band at 1512 cm^{-1} in Raman is assigned to mode 19a. Medium intense band at 1414 cm^{-1} in IR spectra is assigned to mode 19b. Vibration 14 occurs as weak band at 1286 cm^{-1} in IR spectrum. In asymmetric trisubstitution, the allowed tangential C–H in plane bending vibrations is 3, 15 and 18b. Medium intense band at 1214 cm^{-1} in IR spectrum is assigned to vibrational mode 3. The strong band at 1159

cm^{-1} in IR spectra is due to vibration 15. Ring puckering mode is observed at 677 cm^{-1} in Raman spectrum for the title compound.

4.4.2 Methyl group vibrations

The title molecule possess four methyl groups, two at the second and fifth position of the aromatic ring and two methyl groups (methyl III and IV) attached to the second carbon atom of the long chain. The asymmetric methyl stretching bands are observed at 2959 and 2966 cm^{-1} in IR and Raman spectra respectively. Methyl symmetric and asymmetric deformation vibrations are expected in the region 1380-1370 cm^{-1} and 1470 − 1440 cm^{-1} [30], which is 1370 cm^{-1} in IR and 1452 cm^{-1} in Raman spectra respectively. Methyl rocking generally appears as a weak, moderate or sometimes strong band in the region 1050±30 cm^{-1} and 975±45 cm^{-1} [100], which is observed at 1049 cm^{-1} in IR and 937 cm^{-1} in Raman spectra. Methyl torsion mode is expected below 400 cm^{-1} and is observed at 189 cm^{-1} in Raman spectra.

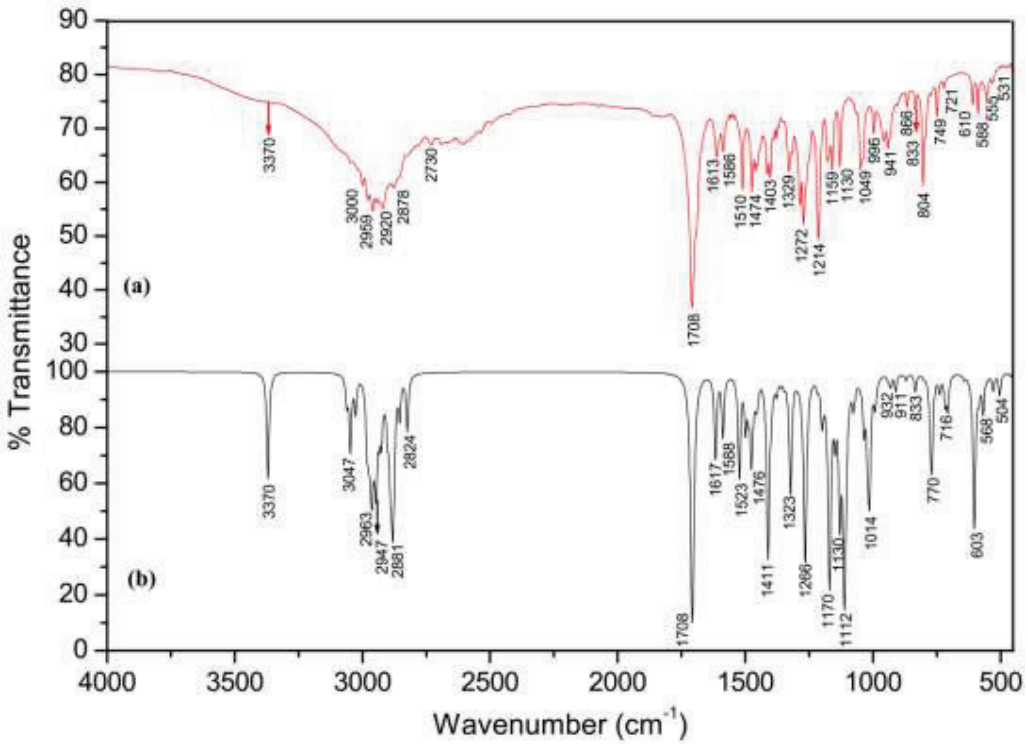

Fig. 4.2 (a) Experimental and (b) Simulated IR spectra of gemfibrozil.

The asymmetric and symmetric stretching vibrations of CH_3 groups (methyl I and II) attached to the benzene ring are usually downshifted due to electronic effects [101] and are expected near 2925 and 2865 cm^{-1} respectively. The asymmetric stretching mode is observed as a weak band at 2920 cm^{-1} in IR and symmetric stretching mode is observed at 2881 cm^{-1} in Raman. Methyl asymmetric and symmetric deformation vibrations of the methyl substituted benzene derivatives normally appear in the region 1440 − 1465 cm^{-1} and 1370 − 1390 cm^{-1} respectively [102, 103]. Methyl symmetric mode is observed at 1388 cm^{-1} in IR and at 1378 cm^{-1} in both IR and Raman spectra. The band at 957 cm^{-1} in IR spectra is assigned to methyl rocking mode. Vibrations corresponding to the C−CH_3 stretching appear as medium intense band at 1174 cm^{-1} in Raman. Bands at 555 and 534 cm^{-1} in IR and Raman are assigned to the C−CH_3 gauche and bending mode respectively.

Table 4.5 Definition of local symmetry coordinates (much like the natural internal coordinates) and the corresponding force constant (mdyne/A°) of gemfibrozil with scale factors used.

No	Symbol	Definition	Scale factors	Force constants (mdyne/Å)
Stretching				
1-6	Ph[νCC]	R_1, R_2, R_3, R_4, R_5, R_6	0.956	6.951
7-9	Ph[νCH]	r_7, r_8, r_9	0.911	5.156
10	Me1[νCC]	r_{10}	1.086	5.130
11	Me2[νCC]	r_{11}	1.086	5.187
12-15	CH_{3ss}	$(r_{12}+r_{13}+r_{14})/\sqrt{3}$, $(r_{15}+r_{16}+r_{17})/\sqrt{3}$, $(r_{18}+r_{19}+r_{20})/\sqrt{3}$, $(r_{21}+r_{22}+r_{23})/\sqrt{3}$	0.898	4.849
16-19	CH_{3ips}	$(2r_{12}-r_{13}-r_{14})/\sqrt{6}$, $(2r_{15}-r_{16}-r_{17})/\sqrt{6}$, $(2r_{18}-r_{19}-r_{20})/\sqrt{6}$, $(2r_{21}-r_{22}-r_{23})/\sqrt{6}$	0.898	4.730
20-23	CH_{3ops}	$(r_{13}-r_{14})/\sqrt{2}$, $(r_{16}-r_{17})\sqrt{2}$, $(r_{19}-r_{20})\sqrt{2}$, $(r_{22}-r_{23})\sqrt{2}$	0.898	4.699
24-26	CH_{2ss}	$(r_{24}+r_{25})/\sqrt{2}$, $(r_{26}+r_{27})\sqrt{2}$, $(r_{28}+r_{29})\sqrt{2}$	0.885	4.618
27-29	CH_{2ips}	$(r_{24}-r_{25})/\sqrt{2}$, $(r_{26}-r_{27})\sqrt{2}$, $(r_{28}-r_{29})\sqrt{2}$	0.898	4.599

No	Symbol	Definition	Scale factors	Force constants (mdyne/Å)
30	Ph[νCO]	Q_{30}	0.956	6.034
31	Mn1[νCC]	R_{31}	0.870	3.918
32	Mn2[νCC]	R_{32}	0.870	3.765
33	Mn3[νCC]	R_{33}	0.870	3.544
34	Mn1[νOC]	Q_{34}	0.898	4.615
35	CC_{3ss}	$(R_{35}+R_{36}+R_{37})/\sqrt{3}$	0.898	4.114
36	CC_{3ips}	$(2R_{35}-R_{36}-R_{37})/\sqrt{6}$	0.898	3.515
37	CC_{3ops}	$(R_{36}-R_{37})/\sqrt{2}$	0.898	3.632
38	νCO	R_{38}	0.911	5.403
39	ν(C=O)	Q_{39}	0.862	11.616
40	νOH	P_{40}	0.836	6.366
Bending				
41-43	Ph[δCH]	$(\beta_{41}-\beta_{42})/\sqrt{2}$, $(\beta_{43}-\beta_{44})/\sqrt{2}$, $(\beta_{45}-\beta_{46})/\sqrt{2}$,	0.914	0.515
44	Ph_{trid}	$(\delta_{47}-\delta_{48}+\delta_{49}-\delta_{50}+\delta_{51}-\delta_{52})/\sqrt{6}$	0.870	1.166
45	Ph_{asyd}	$(2\delta_{47}-\delta_{48}-\delta_{49}+2\delta_{50}-\delta_{51}-\delta_{52})/\sqrt{12}$	0.870	1.225
46	Ph_{asydo}	$(\delta_{47}-\delta_{48}+\delta_{50}-\delta_{51})/2$	0.870	1.173
47-48	Me[δCC]	$(\alpha_{53}-\alpha_{54})/\sqrt{2}$, $(\alpha_{55}-\alpha_{56})/\sqrt{2}$	0.947	0.861
49-52	CH_{3sd}	$(\alpha_{57}+\alpha_{58}+\alpha_{59}-\beta_{69}-\beta_{70}-\beta_{71})/\sqrt{6}$, $(\alpha_{60}+\alpha_{61}+\alpha_{62}-\beta_{72}-\beta_{73}-\beta_{74})/\sqrt{6}$, $(\alpha_{63}+\alpha_{64}+\alpha_{65}-\beta_{75}-\beta_{76}-\beta_{77})/\sqrt{6}$, $(\alpha_{66}+\alpha_{67}+\alpha_{68}-\beta_{78}-\beta_{79}-\beta_{80})/\sqrt{6}$	1.035	0.553
53-56	CH_{3ipb}	$(2\alpha_{57}-\alpha_{58}-\alpha_{59})/\sqrt{6}$, $(2\alpha_{60}-\alpha_{61}-\alpha_{62})/\sqrt{6}$, $(2\alpha_{63}-\alpha_{64}-\alpha_{65})/\sqrt{6}$, $(2\alpha_{66}-\alpha_{67}-\alpha_{68})/\sqrt{6}$	0.925	0.562
57-60	CH_{3opb}	$(\alpha_{58}-\alpha_{59})/\sqrt{2}$, $(\alpha_{61}-\alpha_{62})/\sqrt{2}$, $(\alpha_{64}-\alpha_{65})/\sqrt{2}$, $(\alpha_{67}-\alpha_{68})/\sqrt{2}$	1.035	0.563
61-64	CH_{3ipr}	$(2\beta_{69}-\beta_{70}-\beta_{71})/\sqrt{6}$, $(2\beta_{72}-\beta_{73}-\beta_{74})/\sqrt{6}$, $(2\beta_{75}-\beta_{76}-\beta_{77})/\sqrt{6}$, $(2\beta_{78}-\beta_{79}-\beta_{80})/\sqrt{6}$	0.925	0.650
65-68	CH_{3opr}	$(\beta_{70}-\beta_{71})/\sqrt{2}$, $(\beta_{73}-\beta_{74})/\sqrt{2}$, $(\beta_{76}-\beta_{77})/\sqrt{2}$, $(\beta_{79}-\beta_{80})/\sqrt{2}$	1.014	0.707
69	CC_{3sd}	$(\alpha_{81}+\alpha_{82}+\alpha_{83}-\beta_{84}-\beta_{85}-\beta_{86})/\sqrt{6}$	1.035	1.088
70	CC_{3ipb}	$(2\alpha_{81}-\alpha_{82}-\alpha_{83})/\sqrt{6}$	0.925	1.094
71	CC_{3opb}	$(\alpha_{82}-\alpha_{83})/\sqrt{2}$	1.035	1.122
72	CC_{3ipr}	$(2\beta_{84}-\beta_{85}-\beta_{86})/\sqrt{6}$	0.925	1.088

No	Symbol	Definition	Scale factors	Force constants (mdyne/Å)
73	CC_{3opr}	$(\beta_{85}- \beta_{86})/\sqrt{2}$	1.014	1.241
74	Ph[δCO]	$(\beta_{87}- \beta_{88})/\sqrt{2}$	1.035	1.412
75	Mn1[δOC]	β_{89}	1.035	1.472
76-78	CH_{2sci}	$(5\alpha_{90}+\gamma_{93})/\sqrt{26}$, $(5\alpha_{91}+\gamma_{94})/\sqrt{26}$, $(5\alpha_{92}+\gamma_{95})/\sqrt{26}$	0.947	0.819
79-81	CC_{sci}	$(\alpha_{90}+5\gamma_{93})/\sqrt{26}$, $(\alpha_{91}+5\gamma_{94})/\sqrt{26}$, $(\alpha_{92}+5\gamma_{95})/\sqrt{26}$	0.870	1.301
82-84	CH_{2roc}	$(\beta_{96}-\beta_{97}+\beta_{98}-\beta_{99})/\sqrt{4}$, $(\beta_{100}-\beta_{101}+\beta_{102}-\beta_{103})/\sqrt{4}$, $(\beta_{104}-\beta_{105}+\beta_{106}-\beta_{107})/\sqrt{4}$	0.947	0.864
85-87	CH_{2wag}	$(\beta_{96}+\beta_{97}-\beta_{98}-\beta_{99})/\sqrt{4}$, $(\beta_{100}+\beta_{101}-\beta_{102}-\beta_{103})/\sqrt{4}$, $(\beta_{104}+\beta_{105}-\beta_{106}-\beta_{107})/\sqrt{4}$	0.988	0.683
88-90	CH_{2twi}	$(\beta_{96}-\beta_{97}-\beta_{98}+\beta_{99})/\sqrt{4}$, $(\beta_{100}-\beta_{101}-\beta_{102}+\beta_{103})/\sqrt{4}$, $(\beta_{104}-\beta_{105}-\beta_{106}+\beta_{107})/\sqrt{4}$	0.984	0.681
91	CO_{ipb}	$(\Phi_{108}-\Phi_{109})/\sqrt{2}$	1.035	1.384
92	δOCC	$(2\Phi_{110}-\Phi_{108}-\Phi_{109})/\sqrt{6}$	1.014	1.107
93	δOH	α_{111}	0.988	0.768
Out-of-plane bending (wagging)				
94-96	Ph[gCH]	ω_{112}, ω_{113}, ω_{114}	0.914	0.427
97-98	Me[gCC]	ω_{115}, ω_{116}	0.914	0.529
99	Ph[gCO]	ω_{117}	0.984	0.715
100	gCO	ω_{118}	0.984	0.638
		Torsion		
101	Ph_{puck}	$(\tau_{119}-\tau_{120}+\tau_{121}-\tau_{122}+\tau_{123}-\tau_{124})/\sqrt{6}$	0.914	0.350
102	Ph_{asyt}	$(\tau_{119}-\tau_{121}+\tau_{122}-\tau_{124})/2$	0.914	0.295
103	Ph_{asyto}	$(-\tau_{119}+2\tau_{120}-\tau_{121}-\tau_{122}+2\tau_{123}-\tau_{124})/\sqrt{12}$	0.914	0.317
104-107	τCH_3	$(\tau_{125}+ \tau_{126}+ \tau_{127}+ \tau_{128}+ \tau_{129}+ \tau_{130})/\sqrt{6}$, $(\tau_{131}+ \tau_{132}+ \tau_{133}+ \tau_{134}+ \tau_{135}+ \tau_{136})/\sqrt{6}$, $(\tau_{137}+ \tau_{138}+ \tau_{139}+ \tau_{140}+ \tau_{141}+ \tau_{142}+ \tau_{143}+ \tau_{144}+ \tau_{145})/3$, $(\tau_{146}+ \tau_{147}+ \tau_{148}+ \tau_{149}+ \tau_{150}+ \tau_{151}+ \tau_{152}+ \tau_{153}+ \tau_{154})/3$	0.922	0.007
108	τCC_3 (carboxylic)	$(\tau_{155}+ \tau_{156}+ \tau_{157}+ \tau_{158}+ \tau_{159}+ \tau_{160}+ \tau_{161}+ \tau_{162}+ \tau_{163})/3$	0.906	0.018
109	Ph[τOC]	$(\tau_{164}+ \tau_{165})/\sqrt{2}$	0.906	0.049
110-112	τCH_2	$(\tau_{166}+ \tau_{167}+ \tau_{168})/\sqrt{3}$, $(\tau_{169}+ \tau_{170}+ \tau_{171}+ \tau_{172}+ \tau_{173}+ \tau_{174})/\sqrt{6}$, $(\tau_{175}+$	0.922	0.010

No	Symbol	Definition	Scale factors	Force constants (mdyne/Å)
		$\tau_{176}+\tau_{177}+\tau_{178}+\tau_{179}+\tau_{180})/\sqrt{6}$,		
113	τCO	$(\tau_{181}+\tau_{182}+\tau_{183}+\tau_{184}+\tau_{185}+\tau_{186})/\sqrt{6}$	0.906	0.011
114	τOH	$(\tau_{187}+\tau_{188})/\sqrt{2}$	0.906	0.089

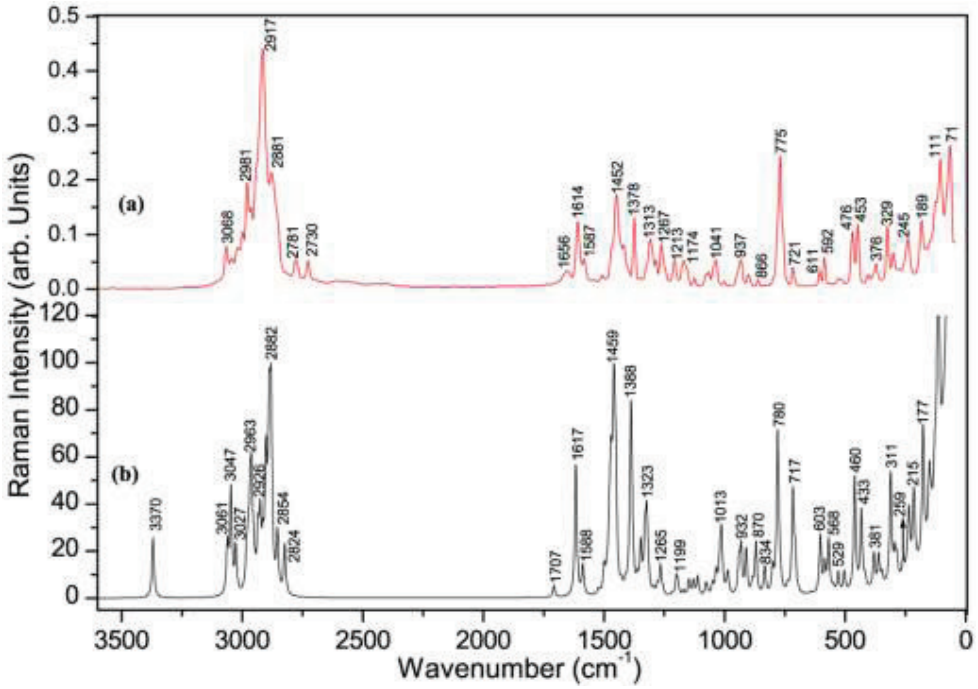

Fig. 4.3 (a) Experimental and (b) Simulated Raman spectra of gemfibrozil.

4.4.3 Methylene group vibrations

The asymmetric CH_2 stretching vibrations are observed as strong intense band at 2917 cm^{-1} in Raman. The medium intense band at 2881 cm^{-1} in IR is assigned to symmetric stretching vibration. The four bending vibrations of CH_2 groups are scissoring, rocking, wagging and twisting. The band at 1474 cm^{-1} in IR is assigned to CH_2 scissoring. Band at 1288 cm^{-1} in Raman spectra is assigned to CH_2 wagging mode. The methylene rocking mode is observed at 721 cm^{-1} in Raman spectrum. The CH_2 twisting mode is observed at 1272 cm^{-1} in IR spectra. In the present study, the CH_2 bending modes follow an order in decreasing wavenumber which is CH_2 scissoring > CH_2 wagging > CH_2 twisting > CH_2 rocking.

4.4.4 Carboxylic acid group vibrations

Vibrational analysis of carboxylic acid is made on the basis of carbonyl and hydroxyl groups. The O−H stretching band is observed as a broad, shallow peak in the region 3500 to 2500 cm^{-1} [101] in IR spectra. This band appears broad and red shifted around 2950 cm^{-1} due to the presence of intermolecular (O−H···O) hydrogen bonding. In theory, this band appears as strong and intense band at 3370 cm^{-1} owing to ignorance of intermolecular contact. As expected very sharp band at 1708 cm^{-1} in IR spectrum is assigned to C=O stretching vibration and which exactly coincides with the theoretical value. Medium intense band at 610 and 611 cm^{-1} in IR and Raman spectra is assigned to torsion mode of hydroxyl group. The wagging of carbonyl (CO) group is observed as medium intense band at 749 cm^{-1} in IR spectra. The stretching frequency of C−O group attached to the phenyl ring is significantly enhanced at 1174 cm^{-1} in Raman spectra and this is due to the conjugation with the ring π system.

Table 4.6 Vibrational assignment of gemfibrozil by normal coordinate analysis based on SQM force field calculations.

Calculated (DFT)			Observed (cm^{-1})		Assignment (% PED, internal coordinates having contribution ≥10% are shown)
υ_{Scaled} (cm^{-1})	IR intensities (%)	Raman intensities (%)	FT-IR	FT-Raman	
3370	21.04	0.33	3370	-	νOH(100)
3061	4.55	0.26	-	3068	Ph[νCH(99)]
3047	13.90	0.56	-	3045	Ph[νCH(99)]
3027	6.13	0.25	-	3022	Ph[νCH(99)]
2982	10.64	0.18	-	2981	Me3[CH_{3ips}(87)] + Me3[CH_{3ops}(11)]
2975	9.05	0.20	2978	-	Me4[CH_{3ops}(70)] + Me4[CH_{3ips}(27)]
2968	11.13	0.35	-	2966	Me3[CH_{3ops}(81)]
2963	10.44	0.24	-	-	Me2[CH_{3ips}(98)]
2962	7.82	0.25	-	-	Me1[CH_{3ops}(68)] + Me1[CH_{3ips}(27)]

Calculated (DFT)			Observed (cm^{-1})		Assignment (% PED, internal coordinates having contribution ≥10% are shown)
υ_{Scaled} (cm^{-1})	IR intensities (%)	Raman intensities (%)	FT-IR	FT-Raman	
2953	8.07	0.18	2959	-	Me4[CH_{3ips}(70)] + Me4[CH_{3ops}(26)]
2946	19.90	0.02	2944	-	Mn2[CH_{2ips}(77)] + Mn3[CH_{2ips}(15)]
2935	7.38	0.28	-	-	Me2[CH_{3ops}(100)]
2926	9.56	0.35	2920	-	Me1[CH_{3ips}(72)] + Me1[CH_{3ops}(28)]
2915	1.49	0.19	-	2917	Mn3[CH_{2ips}(78)] + Mn2[CH_{2ips}(15)]
2902	7.82	0.64	-	-	Me3[CH_{3ss}(84)]
2893	8.79	0.22	-	-	Me4[CH_{3ss}(89)]
2888	12.88	0.70	-	-	Me2[CH_{3ss}(98)]
2881	12.85	0.14	-	-	Mn1[CH_{2ips}(79)] + Mn2[CH_{2ss}(18)]
2881	16.75	0.72	-	2881	Me1[CH_{3ss}(95)]
2876	8.01	0.11	-	-	Mn2[CH_{2ss}(75)] + Mn1[CH_{2ips}(16)] +
2854	6.44	0.31	-	-	Mn3[CH_{2ss}(87)]
2824	9.71	0.27	2824	-	Mn1[CH_{2ss}(98)]
1708	100	0.06	1708	-	ν(C=O)(75)
1617	15.71	0.71	-	1612	Ph[νCC(64)] + Ph[δCH(13)]
1587	11.07	0.16	1586	-	Ph[νCC(69)]
1523	20.20	0.03	-	1512	Ph[νCC(36)] + Ph[δCH(27)] + Mn1[CH_{2sci}(10)]
1500	8.90	0.13	1510	-	Mn1[CH_{2sci}(71)]
1488	4.78	0.08	1492	-	Me3[CH_{3opb}(31)] + Me4[CH_{3opb}(27)] + Me4[CH_{3ipb}(12)]
1478	3.77	0.18	1474	-	Mn2[CH_{2sci}(63)]
1475	11.99	0.10	-	-	Me2[CH_{3ipb}(24)] + Me1[CH_{3opb}(23)] + Mn2[CH_{2sci}(13)]
1471	2.45	0.47	-	-	Me4[CH_{3opb}(33)] + Me4[CH_{3ipb}(26)] +

Calculated (DFT)			Observed (cm^{-1})		Assignment (% PED, internal coordinates having contribution ≥10% are shown)
υ_{Scaled} (cm^{-1})	IR intensities (%)	Raman intensities (%)	FT-IR	FT-Raman	
					Mn2[CH_{2sci}(11)]
1467	1.03	0.08	-	-	Mn3[CH_{2sci}(58)] + Me3[CH_{3ipb}(22)]
1461	0.70	0.46	1471	-	Me3[CH_{3opb}(32)] + Me4[CH_{3opb}(18)] + Me4[CH_{3ipb}(18)] + Me3[CH_{3ipb}(15)]
1459	0.67	0.31	-	-	Me2[CH_{3ipb}(48)] + Me1[CH_{3opb}(29)] +
1456	2.60	0.38	1460	-	Me1[CH_{3ipb}(72)] + Me1[CH_{3opb}(19)]
1452	1.87	0.38	-	-	Me2[CH_{3opb}(89)]
1450	0.44	0.09	-	1452	Me3[CH_{3ipb}(33)] + Me4[CH_{3ipb}(29)] + Mn3[CH_{2sci}(16)]
1427	0.03	0.04	1430	-	Mn1[CH_{2wag}(43)] + Ph[νCC(12)]
1411	47.56	0.04	1414	-	Ph[νCC(24)] + Mn1[CH_{2wag}(23)] + Ph[δCH(16)]
1398	3.09	0.02	1403	-	Mn3[CH_{2wag}(36)] + Me3[CH_{3sd}(21)] + Me4[CH_{3sd}(19)]
1389	0.52	0.88	1388	-	Me2[CH_{3sd}(71)] + Me1[CH_{3sd}(14)]
1385	0.03	0.24	1378	1378	Me1[CH_{3sd}(69)] + Me2[CH_{3sd}(12)]
1377	2.47	0.03	1370	-	Me3[CH_{3sd}(55)] + Mn3[CH_{2wag}(19)]
1361	0.86	0.06	-	-	Me4[CH_{3sd}(58)] + Me3[CH_{3sd}(15)]
1348	1.26	0.25	1352	-	Mn3[CH_{2twi}(40)] + Mn2[CH_{2twi}(12)] + Me4[CH_{3sd}(12)]
1330	1.83	0.29	1329	-	Mn2[CH_{2twi}(30)] + δOH(18) + Mn1[CH_{2twi}(14)]
1323	23.46	0.38	1318	-	Ph[νCC(73)]
1317	0.93	0.08	-	1313	Mn2[CH_{2twi}(35)] + δOH(15) + Mn3[CH_{2twi}(14)]

Calculated (DFT)			Observed (cm^{-1})		Assignment (% PED, internal coordinates having contribution ≥10% are shown)
υ_{Scaled} (cm^{-1})	IR intensities (%)	Raman intensities (%)	FT-IR	FT-Raman	
1295	0.69	0.03	-	1288	Mn2[CH_{2wag}(45)] + Mn3[CH_{2wag}(27)] +
1279	2.00	0.05	-	-	Ph[δCH(70)]
1265	49.00	0.16	1286	-	Ph[νCC(56)] + Ph[νCO(11)]
1256	1.40	0.03	1272	-	Mn1[CH_{2twi}(22)] + Mn2[CH_{2twi}(16)] + δOH(11)
1217	1.26	0.01	1214	-	Ph[δCH(37)] + Me2[νCC](22) + Ph_{trid}(14) + Ph[νCC(10)]
1200	7.07	0.10	1178	-	Mn1[CH_{2roc}(18)] + Mn1[CH_{2twi}(13)]
1193	1.54	0.05	-	-	Me3[CH_{3opr}(21)] + Mn2[νCC(17)] + Me4[CH_{3ipr}(14)] + CC_{3sd}(13)
1170	64.56	0.03	-	1174	Ph[νCO(28)] + Ph[δCH(23)] + Me1[νCC](13) + Ph[νCC(12)]
1148	8.38	0.08	-	-	Me3[CH_{3ipr}(29)] + CC_{3ops}(19)
1130	30.77	0.08	1159	-	Ph[δCH(47)] + Ph[νCC(18)]
1112	81.34	0.11	1130	1130	νCO(40) + δOH(19)
1077	3.91	0.06	-	1082	Me4[CH_{3opr}(22)] + Mn3[CH_{2twi}(13)] + Mn1[CH_{2roc}(13)] + Mn2[CH_{2roc}(10)]
1071	1.16	0.01	1065	-	Me2[CH_{3opr}(77)]
1050	0.53	0.06	-	-	Me1[CH_{3opr}(59)] + Me1[CH_{3ipr}(13)]
1035	8.67	0.12	1049	-	Me3[CH_{3opr}(25)] + Me4[CH_{3ipr}(15)] + Mn1[νCC(10)]
1021	12.59	0.16	-	1041	Me1[CH_{3ipr}(39)] + Mn1[νOC(18)] + Ph[νCC(10)]
1014	21.16	0.19	-	1006	Mn1[νOC(43)] + Me1[CH_{3ipr}(18)]

Calculated (DFT)			Observed (cm^{-1})		Assignment (% PED, internal coordinates having contribution ≥10% are shown)
υ_{Scaled} (cm^{-1})	IR intensities (%)	Raman intensities (%)	FT-IR	FT-Raman	
1012	3.83	0.16	-	-	Mn1[νCC(60)] + Mn2[νCC(10)]
992	4.10	0.02	996	-	Me2[CH_{3ipr}(26)] + Mn2[νCC(22)]
986	1.40	0.11	957	-	Mn2[νCC(31)] + Me2[CH_{3ipr}(25)]
941	0.70	0.17	-	937	Me4[CH_{3ipr}(16)] + CC_{3ops}(16) + Me4[CH_{3opr}(16)]
932	1.99	0.24	-	906	Ph[νCC(20)]
911	2.82	0.24	866	866	Me3[CH_{3ipr}(18)] + CC_{3ips}(13) + CC_{3ops}(12)
884	0.13	0.06	-	840	Ph[gCH(92)]
870	1.07	0.28	833	-	Mn3[νCC(24)] + Mn1[CH_{2roc}(14)] + Mn3[CH_{2roc}(13)]
834	2.95	0.15	-	817	CC_{3ips}(28) + Mn1[CH_{2roc}(11)] + Mn3[νCC(11)]
800	0.48	0.13	804	-	Ph[gCH(80)]
780	0.92	0.85	795	-	Ph[νCC(36)] + Me2[νCC](22) + Ph_{asydo}(11)
773	9.03	0.08	-	775	Ph[gCH(85)]
769	14.09	0.04	749	-	gCO(48) + τOH(10)
739	2.64	0.04	-	721	Mn2[CH_{2roc}(39)] + Mn3[CH_{2roc}(27)]
717	4.72	0.54	702	-	Ph_{trid}(20) + CC_{3ss}(19) + CO_{ipb}(13)
707	5.69	0.20	-	692	CC_{3ss}(17) + CO_{ipb}(15) + Ph_{trid}(15)
643	0.67	0.01	-	677	Ph_{puck}(48) + Ph[gCO(29)] + Me[gCC(12)]
603	35.57	0.31	610	611	τOH(80)
585	2.93	0.15	-	592	Ph_{asyd}(33) + Mn1[CC_{sci}(11)]
568	6.40	0.29	588	-	δOCC(12) + Mn1[δOC(12)] + CC_{3ss}(10)

Calculated (DFT)			Observed (cm^{-1})		Assignment (% PED, internal coordinates having contribution ≥10% are shown)
υ_{Scaled} (cm^{-1})	IR intensities (%)	Raman intensities (%)	FT-IR	FT-Raman	
549	0.49	0.03	555	-	Ph_{puck}(33) + Me[gCC(27)] + Ph_{asyt}(17) + Ph[gCH(11)]
529	2.69	0.11	-	534	Ph[δCO(21)] + Me[δCC(20)]
504	3.59	0.11	497	-	CO_{ipb}(26) + δOCC(16) + CC_{3opb}(10)
461	0.53	0.62	-	476	Ph_{asydo}(34) + Mn3[CC_{sci}(13)]
433	1.34	0.43	-	453	Ph_{asydo}(19) + Ph_{asyd}(17) + CC_{3opr}(14) + Mn3[CC_{sci}(12)]
417	0.76	0.06	-	410	Ph_{asyto}(47) + Me[gCC(25)]
381	0.63	0.19	-	376	Me[δCC(17)] + CC_{3sd}(13) + Mn2[CC_{sci}(12)]
361	0.29	0.17	-	-	Me[δCC(21)] + CC_{3sd}(15) + CC_{3ipb}(14) + Ph_{asyd}(11) + Mn1[δOC(11)]
347	1.34	0.06	-	329	CC_{3ipb}(34) + CC_{3ipr}(16) + CC_{3opr}(13)
311	0.01	0.60	-	304	Me[gCC(55)] + Ph_{asyt}(17) + Ph[gCH(10)]
294	0.57	0.15	-	-	Me[δCC(41)]
285	0.34	0.11	-	-	Me[δCC(30)] + CC_{3ipb}(11)
259	0.08	0.10	-	-	Me4[τCH_3(26)] + Me3[τCH_3(23)]
241	0.16	0.10	-	245	CC_{3opb}(44) + CC_{3opr}(10)
235	0.05	0.30	-	-	Me4[τCH_3(34)]
217	0.01	0.25	-	-	Ph_{asyt}(25) + Ph_{puck}(14) + Ph[gCH(14)] + Me3[τCH_3(11)]
213	0.03	0.22	-	189	Me3[τCH_3(36)] + Me4[τCH_3(22)] + Ph_{asyt}(12)
177	0.06	0.68	-	171	Mn2[CC_{sci}(16)] + CC_{3sd}(11) + Me[δCC(10)]
151	0.25	0.33	-	-	Me2[τCH_3(63)]
144	0.78	0.11	-	-	Ph[τOC(19)] +

Calculated (DFT)			Observed (cm^{-1})		Assignment (% PED, internal coordinates having contribution ≥10% are shown)
υ_{Scaled} (cm^{-1})	IR intensities (%)	Raman intensities (%)	FT-IR	FT-Raman	
					Mn2[τCH_2(17)] + Me2[τCH_3(17)]
129	0.53	0.24	-	129	Ph_{asyto}(34) + Ph[gCH(15)] + Ph_{asyt}(12) + Me[gCC(10)]
119	0.09	0.47	-	111	Mn3[CC_{sci}(21)] + Ph[τOC(18)]
112	0.01	0.97	-	71	τCC_3(34) + Mn1[τCH_2(17)] + Mn2[τCH_2(13)] + Me3[τCH_3(11)]
60	0.24	3.46	-	-	Ph[τOC(29)] + Mn1[τCH_2(27)] + τCC_3(12)
49	0.02	1.82	-	-	Mn1[CC_{sci}(21)] + Mn2[CC_{sci}(21)] + τCO(17) + Mn1[δOC(11)]
32	0.08	2.52	-	-	Me1[τCH_3(61)] + Me[gCC(23)]
29	0.28	9.68	-	-	τCO(51) + CC_{3sd}(12) + CC_{3ipr}(10)
22	0.01	86.45	-	-	Mn1[τCH_2(39)] + Ph[τOC(35)]
17	0.03	100	-	-	Mn3[τCH_2(33)] + Mn2[τCH_2(19)]

Ph, phenyl ring; Me, Methyl; Mn, Methylene; ν, stretching; δ, bending; τ, torsion; g, gauche; ss, symmetric stretching; ips, in plane stretching; ops, out of plane stretching; ipb, in plane bending; opb, out of plane bending; ipr, in plane rocking; opr, out of plane rocking; wag, wagging; twi, twisting; puck, puckering; trid, trigonal deformation; asyd, asymmetric deformation; asydo, out of plane asymmetric deformation; asyt, asymmetric torsion; asyto, out of plane asymmetric torsion.

4.5 HOMO – LUMO energy gap

The HOMO (highest occupied molecular orbital) – LUMO (lowest unoccupied molecular orbital) energy gap of gemfibrozil has been calculated at the B3LYP/6-31G* level. The eigen values of LUMO and HOMO and their energy gap reflect the

chemical activity of the molecule [104]. The atomic orbital components of the frontier molecular orbitals are shown in Fig. 4.4.

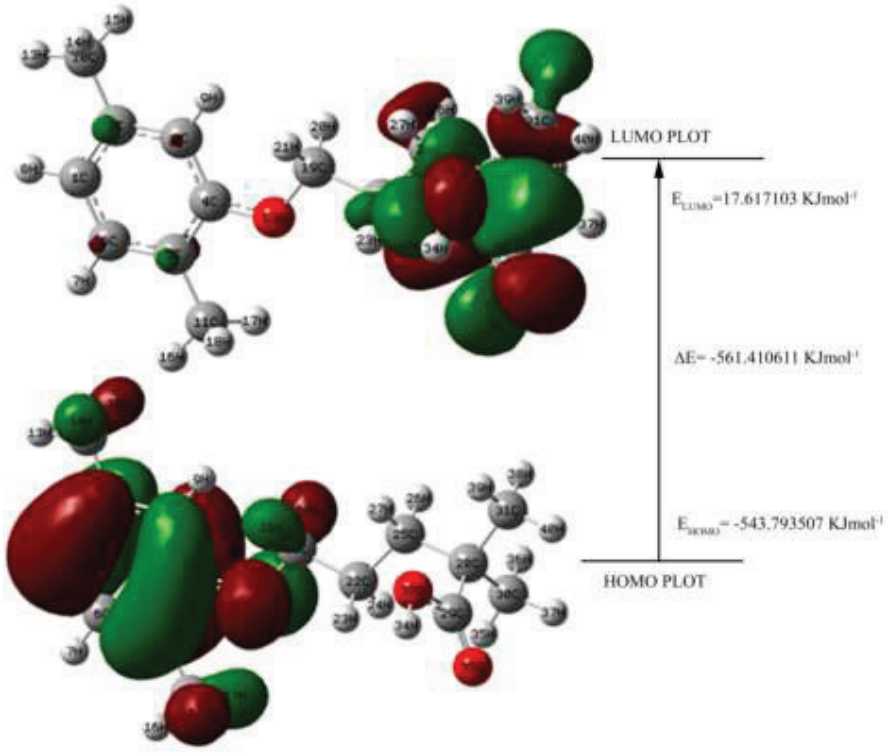

Fig. 4.4 The atomic orbital components of the frontier molecular orbital of gemfibrozil.

HOMO energy = -543.793507 KJmol^{-1}
LUMO energy = 17.617103 KJmol^{-1}
HOMO – LUMO energy gap ΔE = -561.410611 KJmol^{-1}

The HOMO is located over the phenyl ring and the methyl groups attached to the phenyl ring. The HOMO→LUMO transition implies an electron density transfer to the carboxylic acid group from the phenyl ring. Lowering in the HOMO – LUMO energy gap explains the eventual charge transfer interactions taking place within the molecule which is responsible for the bioactivity of the molecule [105]. The calculated self-consistent field (SCF) energy of Gemfibrozil is -810.5450 a.u.

4.6 Mulliken atomic charges

The charge distribution of Gemfibrozil shows that the carbon atom attached with hydrogen atoms is negative, whereas the remaining carbon atoms are positively charged (Table 4.7).

Table 4.7 Atomic charges for optimized geometry of gemfibrozil at B3LYP/6-31G (d) level.

Atom No.	Atomic charge (e)	Atom No.	Atomic charge (e)
C_1	-0.1856	H_{21}	0.1390
C_2	0.1730	C_{22}	-0.2911
C_3	-0.2491	H_{23}	0.1575
C_4	0.3297	H_{24}	0.1568
C_5	0.1228	C_{25}	-0.2719
C_6	-0.1890	H_{26}	0.1352
H_7	0.1185	H_{27}	0.1527
H_8	0.1142	C_{28}	0.0027
H_9	0.1224	C_{29}	0.5926
C_{10}	-0.5298	C_{30}	-0.4438
C_{11}	-0.5125	C_{31}	-0.4566
O_{12}	-0.5284	O_{32}	-0.5803
H_{13}	0.1542	O_{33}	-0.4681
H_{14}	0.1586	H_{34}	0.4087
H_{15}	0.1574	H_{35}	0.1628
H_{16}	0.1450	H_{36}	0.1372
H_{17}	0.1619	H_{37}	0.1594
H_{18}	0.1624	H_{38}	0.1507
C_{19}	-0.0249	H_{39}	0.1639
H_{20}	0.1363	H_{40}	0.1549

The oxygen atoms have more negative charges whereas all the hydrogen atoms have positive charges. The maximum atomic charge is obtained for C_{29} when compared with other atoms. This is due to the attachment of two negatively charged oxygen (O_{32} and O_{33}) atoms. Illustration of atomic charges plotted is shown in Fig.

4.5. Negatively charged lone pair oxygen (O_{12}) atom shows that charge is transferred from O to H ($O_{12}\rightarrow H_{20}$ and $O_{12}\rightarrow H_{21}$). The calculated Mulliken charges of H_{20} (0.136 e), H_{21} (0.139 e) and O_{12} (-0.528 e) taking part in intramolecular charge transfer is revealed in the natural bond orbital analysis. Carbon atoms (C_{10} and C_{11}) are more negatively charged which indicates the charge transfer from H to C.

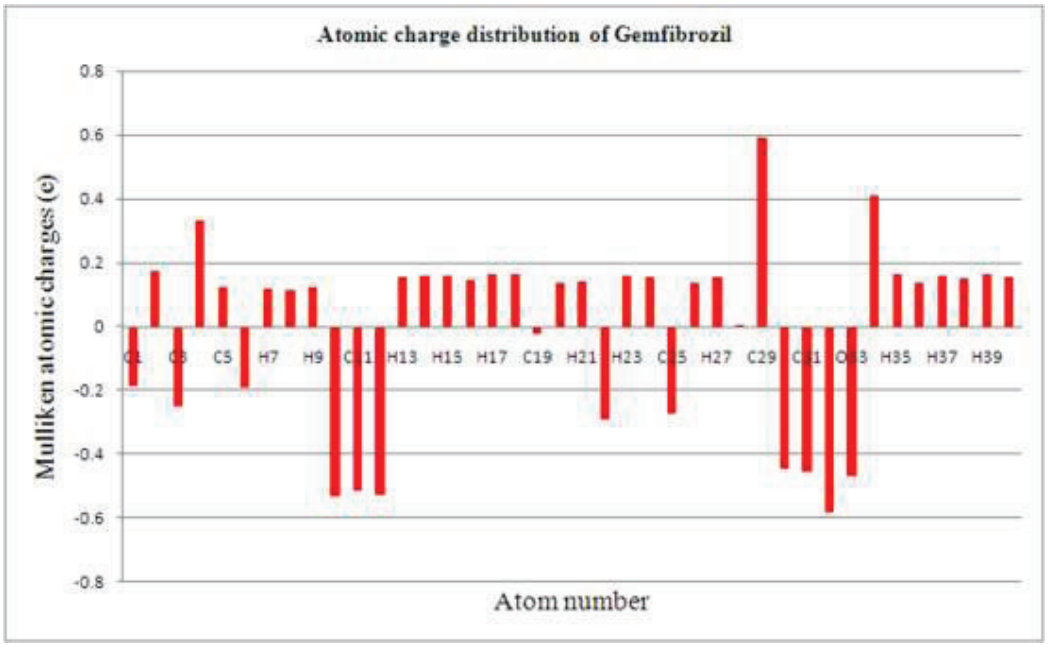

Fig. 4.5 Atomic charge distribution of gemfibrozil.

4.7 Conclusion

Molecular modeling of Gemfibrozil is done at B3LYP/6-31G(d) level. The calculated geometry of the molecule agrees well with the experimental values. NBO analysis clearly demonstrates the two intramolecular interaction ($H_{20}\cdots O_{12}$ and $H_{21}\cdots O_{12}$) and the charge transfer reaction of the methyl groups attached to the phenyl ring. A complete vibrational investigation of the title compound has been performed using FT-IR and Raman spectroscopic techniques. The simulated IR and Raman spectra of the title compound show good agreement with the observed spectra. Scale

factors have been refined with an RMS error of 8.66 cm^{-1} between the experimental and SQM frequencies. Mulliken atomic charge analysis shows that charge transfer occurring within the molecule. Decrease in HOMO and LUMO energy gap explains the eventual charge transfer within the molecule which is responsible for the chemical reactivity of the molecule.